Academic Science Journal

Synthesis and Characterization of Mn_2O_3 Nanoparticles Prepared by Sol-Gel Method

Duaa. N. Jassim[1*], Jassim. M. Mansour[1], Ghuson H. Mohammed[2]

[1]Physics Department, College of Science, University of Diyala, Iraq

[2]Physics Dep., College of Science, University of Baghdad, Baghdad, Iraq

[*] duaam@uodiyala.edu.iq

Received: 5 March 2024 **Accepted: 12 May 2024**

Published: July 2025

DOI: https://dx.doi.org/10.24237/ASJ.03.03.871C

Abstract

The auto-combustion approach of the Sol-Gel Method was employed in this study to synthesize Mn_2O_3 nanoparticles, whereas the applied temperatures were 500 ℃ .Using measurements of its structural properties from X-ray diffraction investigations, the cubic nature of the pure Mn_2O_3 crystal structure was established. The maximum intensity region was further revealed by the diffraction pattern to be at an angle of 2θ=33.1°. Furthermore, the growth pattern that was shown to be predominant was (222) having cubic structure (a=b=c= 9.409A°). Using the Scherrer equation, the crystal size (D) of the X-ray diffraction pattern for each sample was found. Based on the investigation, the Mn_2O_3 sample's average crystal size was approximately 37.18 nm. The Mn_2O_3 field emission scanning electron microscopy (FESEM) micrographs show significant clusters of spherical or semi-spherical grains in some areas of the images, indicating an unequal rate of grain growth. The wavelength range used to measure Mn_2O_3 optical properties was 300–1100 nm. The wavelength where the greatest amount of absorption happens is 500 nm, meaning that it is in the 400–800 nm range of the visible zone. It was found that Mn_2O_3 had a band gap of 1.42 eV.

Keywords: Sol–gel processes; Structural properties.

Introduction

Particle size is a crucial factor in the realm of nanotechnology, as it significantly influences the formation of materials. When a material is of nanoscale dimensions, it holds great significance for researchers due to its diverse features, encompassing optical, structural, and magnetic variables. Metal oxide nanoparticles have garnered significant attention because of their distinct optical, electrical, and magnetic properties, which frequently deviate from those of the bulk material [1]. The characteristics of nanoparticles are affected by various crucial parameters, such as their form, size, composition, and structure [2].

Dimension and form are the regulating elements of nanoparticle size, which in turn contribute to the stable distinguishing properties exhibited by materials. As such, the production of nanoparticles depends on their atomic structure, which is precisely controlled in terms of size [3,4] Scholarly study has focused a lot of attention on the unique electrical and physical properties of large specific surface area metal nanoparticles [5]. Manganese oxide nanoparticles have several applications due to their favorable physico-chemical characteristics. It has been shown that these nanoparticles work remarkably well as batteries, molecular sieves, magnetic materials, and catalysts[6]. They have also been applied in other domains, including as optoelectronics and water purification [7]. One of the main goals of study in the realm of solar cell studies has been to analyze the optical and electrical characteristics of synthetic manganese oxide nanoparticles [8]. Numerous techniques, including femtosecond laser ablation [8], hydrothermal synthesis [9], reflux treatment [10], quick precipitation approach [11], redox method [12], green synthesis [13], precipitation [14], and sol-gel procedure [15], can be used to create manganese oxide nanoparticles.

S. Sharma et al 2016, studied Mn_2O_3 nanoparticles synthesized using chemical co-precipitation method. The as synthesized nanoparticles were characterized by X-ray diffraction (XRD), UV-Visible spectrophotometer (UV-Vis) and Fourier Transform Infra-Red (FTIR) spectrophotometer method. The results indicate that the prepared Mn_2O_3 nanoparticles possessed crystallites having sizes 12.56 nm and 11.90 nm with cubic and orthorhombic structures respectively. The two samples are named as M1 and M2. The gas response of both the samples was investigated for different concentrations of NH3 gas at room temperature.

Sample M2 based thick film sensor showed enhanced sensing performance in comparison to sample M1. This is attributed to smaller crystallite size of sample M2. The sample M2 based sensor showed the response of 67.1% with the response and recovery times 65 and 71 sec respectively. The fabricated nanoparticles show promising use as room temperature NH_3 sensors [16].

This work will synthesize and evaluate Mn_2O_3 nanoparticles utilizing the auto-combustion Sol-Gel technique, highlighting its optical and structural features.

Experimental Parts

Sol-gel, an auto combustion technique, was used to produce manganese oxide nanoparticles. Solution is made by mixing 75 milliliters of distilled water with 5.937 grams of manganese chloride ($MnCl2.4H_2O$) with continuous stirring to dissolve manganese chloride completely and for the twenty minutes. In this procedure, 75 milliliters of distilled water are mixed with a specific amount of 6.304 g of citric acid also with stirring to dissolve ctric acid. Then Equal volumes of citric acid solution to chloride solutions were added, and the mixture was left to react for thirty minutes at 50℃. Citric acid is one of the fuels used in the combustion process. Then the gel is formed at 90℃. When the temperature is raised to 300℃, bubbles form and then turn into ash. The final product was then successfully obtained as a crystalline powder by calcining it for two hours at 500 ℃.

The structural characteristics of Mn_2O_3 nanoparticles were analyzed using a Philips PW1730 X-ray diffractometer. The analysis was conducted using Cu-Kα radiation with a wavelength of 0.15406 nm, and the scan range was set from 10 to 80° in 2θ.The surface topography of the particles was examined using FE-SEM. The UV–Vis-NIR spectrophotometer (Metertech, SP8001) was employed to investigate the optical characteristics of thin films within the wavelength range of (190-1100) nm.

Result and Discussion

The XRD techniques were employed to investigate the structural and crystalline characteristics of the produced nanoparticle samples. Figure 1 presents the X-ray diffraction pattern of Mn_2O_3 NPs nanoparticles that were synthesized using the Sol-gel auto combustion process and subsequently subjected to thermal degradation. All observed peaks can be indexed

to a pure cube structure. The sharp peak of XRD exhibits the prepared samples were highly intensity crystalline in nature at an angle of 2θ˚ = 33.1coresponding to (222) plans having cubic structure (a=b=c= 9.409A°) indicating its dominant growth tendency and its crystallite size is found 38.804 nm. Additionally , the typical XRD patterns also observed other diffraction peaks at 2Θ= 23.31, 28.90, 33.1, 35.7, 38.41,42.52, 44.5, 45.31, 49.4, 50.98, 55.3, 58.7, 60.5, 65.9, 67.56, 69.3 and 73.9 which are corresponding to Braggs reflections from (211), (112), (222), (321), (400), (420), (220), (332), (431), (105), (440), (600), (611), (622), (631), (444) and (721) planes which corresponds to Mn_2O_3NPs nanoparticle diffraction angles (23.31, 33.1, 35.7, 38.41,42.52, 45.31, 49.4, 55.3, 58.7, 60.5, 65.9, 67.56, 69.3 and 73.9). These diffraction peaks correspond to the International Centre for Diffraction Data (ICDD) number (00-041-1442). Also, It is evidenced from the figure that the presence of a distinct phase of manganese oxide (Mn3O4) at planes (112), (220) and (105) as indicated by its corresponding to 2Θ=(28.90, 44.5and 50.98) . The obtained results are in good agreement with the JCPDS reference number (00-001-1127).

The crystal size (D) of the X-ray diffraction pattern for the samples was determined by employing the Scherrer equation [16].

$$D = K\lambda/(B\cos\Theta) \quad (1)$$

Where, $\boldsymbol{\beta}$ is the full width at half maximum (FWHM) of a diffraction peak, K is the shape factor ~ 0.9 ,λ is the wavelength of x -ray source(1.54 Å) and θ is the diffraction angle.

Using the Braggs formula, the intermolecular planar spacing (dhkl) was calculated [17]:

$$n\lambda = 2d_{hkl}\sin\Theta \quad (2)$$

Table 1: Crystallite size and other parameters of Pure Mn_2O_3 Sample

peak position (2θ°)	FWHM β (°)	d-spacing (A°)	Crystallite size D (nm)	Average Crystallite D (nm)
23.31	0.235	3.81	36.038	40.84372847
33.13	0.223	2.70	38.804	
35.7	0.239	2.47	36.519	
38.41	0.186	2.34	47.214	
49.4	0.19960	1.84019	45.738	
55.31	0.244	1.65	38.377	
58.7	0.16470	1.57128	45.738	
60.52	0.200	1.53	47.901	
65.90	0.192	1.41	51.479	

Academic Science Journal

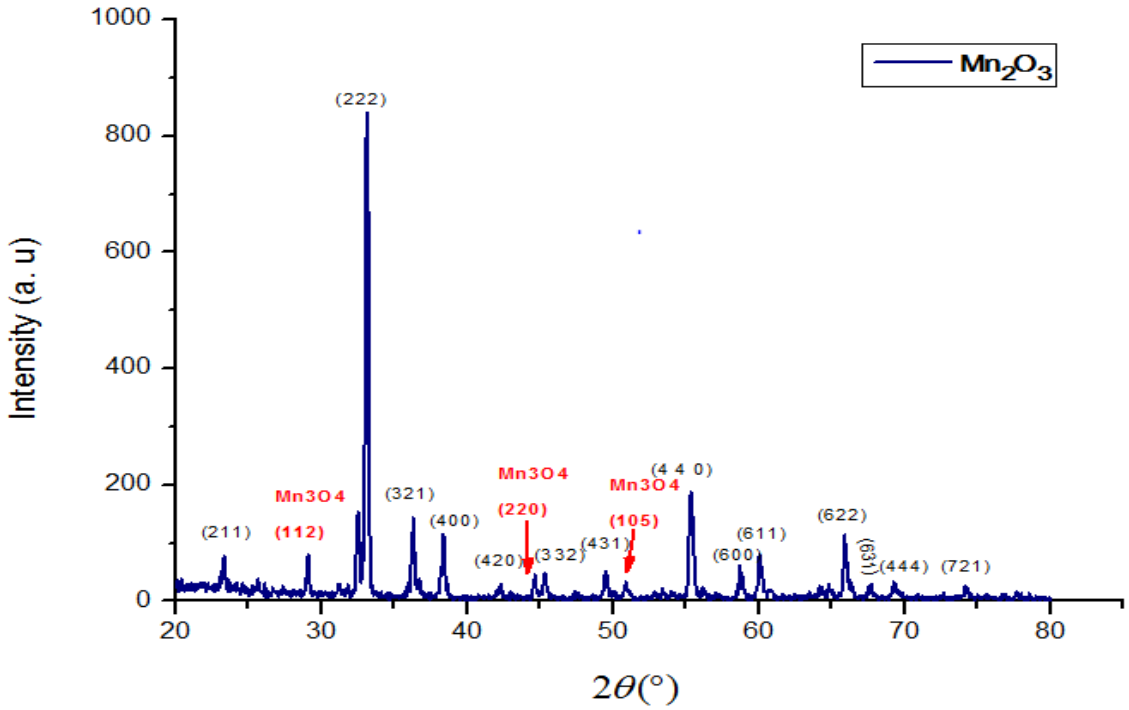

Figure 1: X-ray diffraction pattern of Mn_2O_3 Nanoparticles

The researchers employed the Williamson-Hall (W-H) method to ascertain the dimensions and lattice strain of crystallites based on X-ray diffraction (XRD) data [16]. The equation was utilized to determine the strain induced in powders, which originates from various flaws like as dislocation, twinning, imperfection, and distortion.

$$\varepsilon = \beta_s / 4\tan\Theta \quad (3)$$

The symbol β_s represents the peak broadening resulting from lattice strain, whereas Θ denotes the Bragg's angle. The entire peak broadening βhkl can be mathematically represented using equations (1) and (2).

$$\beta_{hkl} = \beta D + \beta s \quad (4)$$

$$\beta_{hkl} \cos\Theta = (K\lambda / D) + (4\varepsilon \sin\Theta) \quad (5)$$

Equation (4) represents the W-H equation. The figure (2) displays the W-H plot. The plot is constructed with the variable sinΘ on the x-axis and βhkl cosΘ on the y-axis, where βhkl is measured in radians and the points that are distant from the red line in the image represent the (321), (400) , (440) plan. Table 2 presents the strain and grain size values obtained from the

W-H approach, as well as the grain size values obtained from the D-S method, for Mn_2O_3-NPs [18].

Table 2: Strain and particle size data for Mn_2O_3 nanoparticles (NPs) as determined by the W-H and D-S methods.

Sample	D(W-H) nm	ε (W-H)*10^{-4}	D (D-S) nm
Mn_2O_3	45.82797468	3.02553	42.3330286

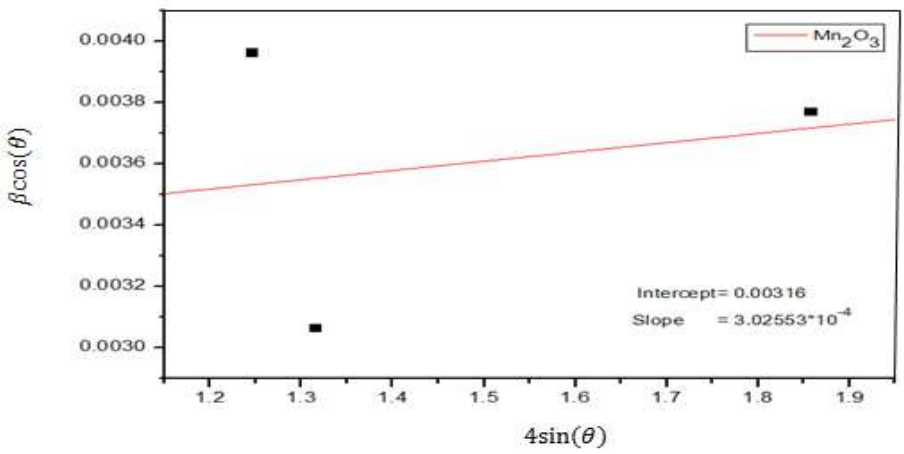

Figure 2: Williamson-Hall results of Mn_2O_3 nanoparticles

The surface morphology of Mn_2O_3 nanoparticles was analyzed using a Field Emission Scanning Electron Microscope (FE-SEM). The observation revealed that the Mn_2O_3 exhibited a high degree of crystallite density. Figure 3 displays the surface photograph image of Mn_2O_3 at $5\mu m$, $4\mu m$ and 200nm which exhibited characteristics of density, smoothness, and non-homogeneity. Additionally, it has been shown that the grains exhibit a combination of nano cauliflower and spherical morphologies, displaying variations in size. The outcome aligns with the findings presented in reference [19].

The photos were subjected to analysis using the software program Image J to determine the average size of the particles. The resulting particle size was found to be 48nm. The field emission scanning electron microscopy (FESEM) micrographs of Mn_2O_3 exhibit the presence of significant agglomerations of spherical or semi-spherical grains in certain regions of the

pictures, suggesting an uneven growth rate of these grains. Furthermore, the photos presented a densely packed arrangement of grains that uniformly covered the whole surface, devoid of any imperfections such as cracks or pinholes.

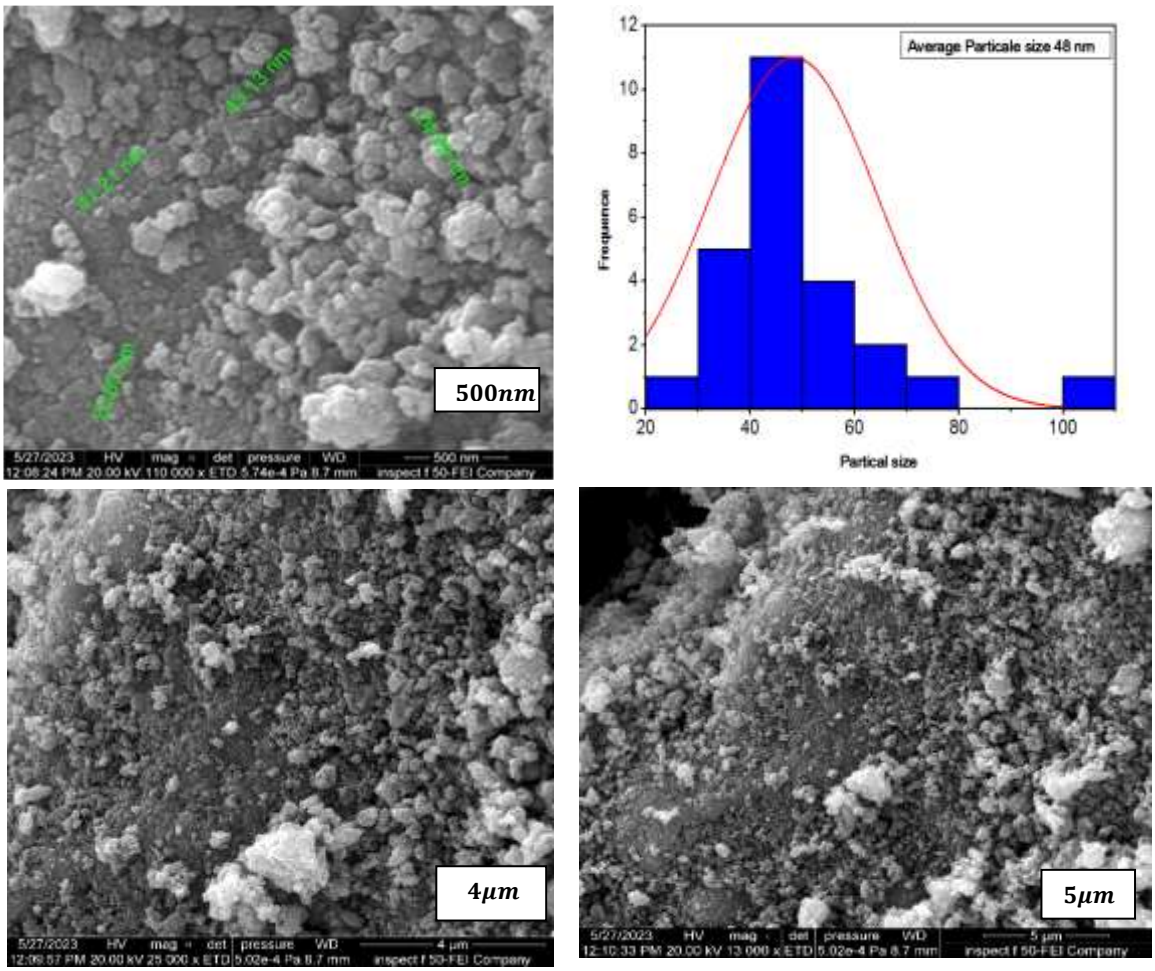

Figure 3: FE-SEM images of Mn_2O_3 nanoparticles

The spectra of Mn2O3 obtained using an Energy Dispersive Spectroscope (EDS) are presented in Figure 4. The quantitative chemical analysis is presented in Table 3. The research provides evidence for the existence of the elements Mn and O. It is of utmost significance to acknowledge that there are no discernible supplementary peaks associated with impurities or contaminants, so affirming the cleanliness of the sample preparation.

Academic Science Journal

Table 3: Mn and O concentration in Mn_2O_3 sample

Element	Atomic %	Atomic % Error	Weight %	Weight % Error
O	**51.3**	**0.5**	**23.5**	**0.2**
Mn	**48.7**	**0.2**	**76.5**	**0.3**

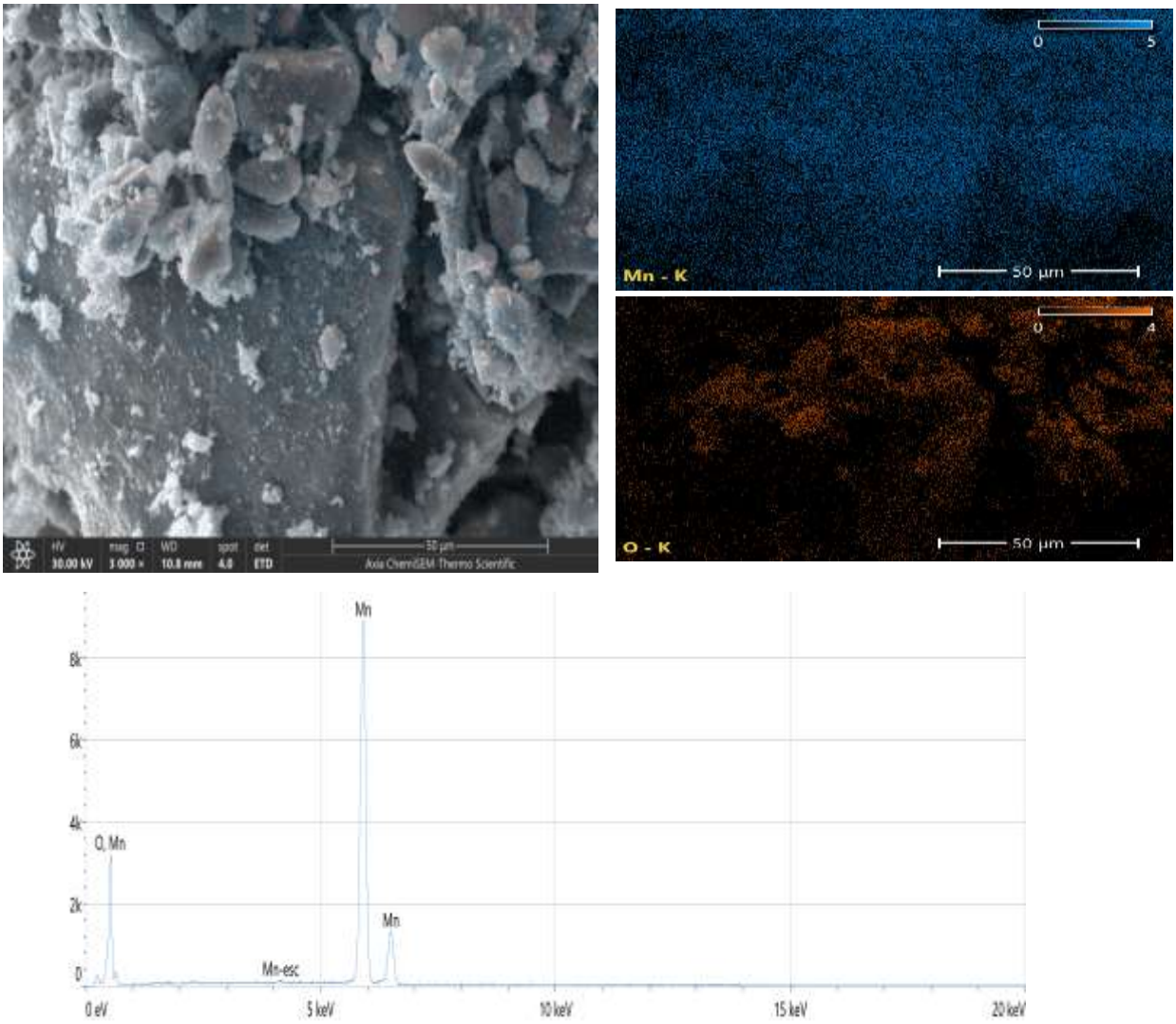

Figure 4: EDS analysis of Mn_2O_3 nanoparticles.

The Fourier Transform Infrared (FT-IR) spectra of the Mn_2O_3NPs material are depicted in Figure 5. The Fourier Transform Infrared (FTIR) spectrum is utilized for the purpose of confirming the bonding properties exhibited by the Mn_2O_3 material. The FTIR spectrum displays six peaks at certain wavenumbers (3425, 1631, 1514, 1394, 1251, 1103, 584, and

572) cm^{-1}, which correspond to different bonding characteristics of the surface absorbed water molecule and Mn_2O_3. The peak observed at the wavenumber of 3425 cm-1 is attributed to the stretching vibration of the hydroxyl (O-H) functional group. The observed peak at 1631,1514 cm^{-1} can be attributed to the adsorption of moisture on the surface of the materials. Additionally, the peaks observed at 1394, 1251, and 1103 cm^{-1} suggest the presence of coupled bending vibrations involving the Mn atoms and O-H groups. The vibrational modes detected at wavenumbers 584 and 572 cm−1 correspond to the stretching movements of tetrahedral and octahedral sites in Mn–O bonds, respectively [20, 21].

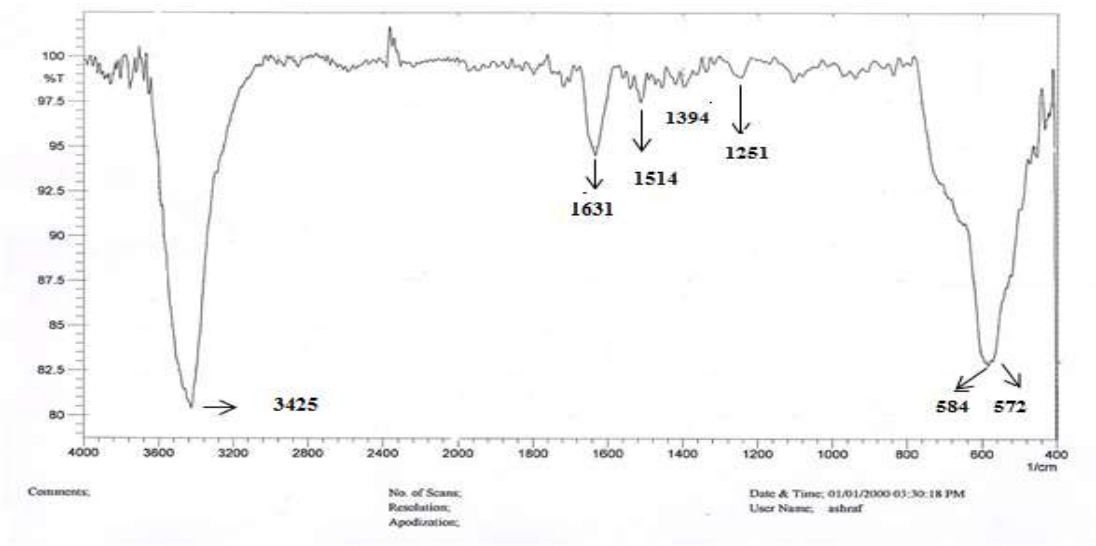

Figure 5: FTIR of Mn_2O_3

The absorbance spectrum of Mn2O3 is depicted in Figure 6, illustrating the relationship between the absorbance with wavelengths in the range from 300 to 1100 nm. It has been observed that the absorbance has an inverse relationship with the transmittance, reaching its maximum value at a wavelength of 500 nm. This indicates that the absorbance falls within the visible region (400-800 nm). This particular absorbance value aligns with the findings presented in reference [22].

Academic Science Journal

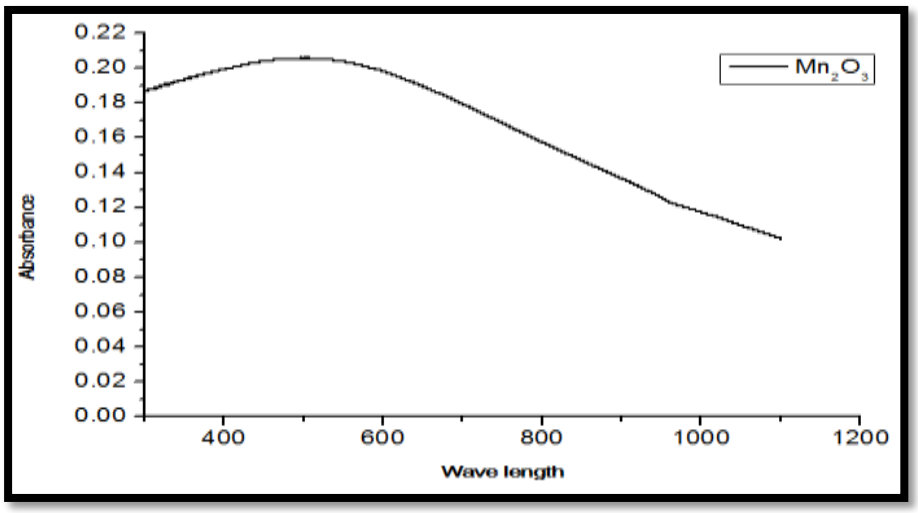

Figure 6: Absorbance versus wavelength of Mn_2O_3

The energy band gap (Eg) of the sample was determined by applying the Tauc and Davis-Mott models, which establish a relationship between the absorption coefficient (α) and the energy of the photon (hv).[23]

$$(ahv)^2 = A(hv - E_g) \quad (6)$$

The value of α is defined as 2.303 A/L, where A represents the absorbance of the sample. The energy band gap, Eg, was determined by identifying the point where the curve $(\alpha hv)^2$ vs. (hv) intersects the y-axis at y = 0, as depicted in the inset of Figure 6. The calculated value for Eg was 1.24 eV [23].

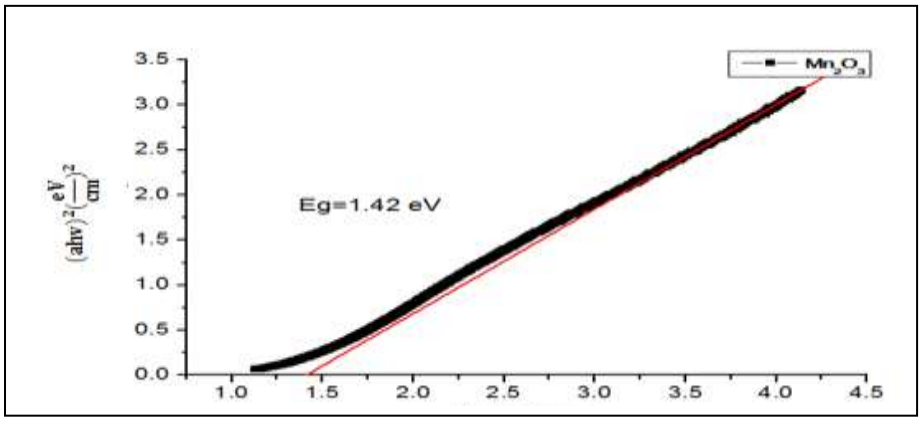

Figure 7: Graphs illustrating the relationship between the square of the product of αhυ and the product of photon Energy for Mn_2O_3 nanoparticles.

Conclusion

The synthesis of Mn_2O_3 nanoparticles has been effectively achieved by the sol-gel process, specifically employing the auto-combustion technique. The cubic structure of Mn_2O_3 was established using X-ray diffraction (XRD) research. The construction of Williamson-Hall plots was undertaken to estimate the lattice constant. The surface morphology of Mn_2O_3 was analyzed using a Field Emission Scanning Electron Microscope (FESEM). The pictures revealed the presence of sizable clusters consisting of spherical or semi-spherical grains in certain areas, suggesting an uneven growth rate of the grains. The objective is to accurately determine the crystallite plot and microstrain. The production of the metal-oxide phase in the manganese oxide nanoparticles was established using FTIR spectrum analyses. The EDX analysis yielded conclusive evidence regarding the existence of manganese (Mn) and oxygen (O) elements. The optical tests revealed that the absorbance reached its maximum value at a wavelength of 500 nm, while the energy gap of Mn_2O_3 was determined to be 1.42 eV.

Source of funding: Funding for the research was self-funded.

Conflict of interest: The authors declare no conflicts of interest.

Ethical clearance: none

References

[1] I. Khan , K. Saeed, and Id. Khan ,Nanoparticles: Properties, applications and toxicities, Arabian Journal of Chemistry, 12(7), 908-931(2019), DOI(https://doi.org/10.1016/j.arabjc.2017.05.011)

[2] T. Mounika, K. Meenu, S. L. Belagali, C. Dharmashekar, K. T. Vadiraj, C. Shivamallu, S. P. Kollur, Ferric oxide quantum dots (FOQDs) for photovoltaic and biological applications: Synthesis and characterization, Inorg Chem Commun, 140, 109487(2022), DOI(https://doi.org/10.1016/j.inoche.2022.109487)

[3] L. Ji, X. Zhang, Evaluation of Si/carbon composite nanofiber-based insertion anodes for new-generation rechargeable lithium-ion batteries, Energy Environ Sci, 3(1), 124–129(2010), DOI(10.1039/b912188a)

[4] L. Qie, W. M. Chen, Z. H. Wang, Q. G. Shao, X. Li, L. X. Yuan, X. L. Hu, W. X. Zhang, Y. H. Huang, Nitrogen-Doped Porous Carbon Nanofiber Webs as Anodes for Lithium Ion Batteries with a Superhigh Capacity and Rate Capability, Adv Mater, 24(15), 2047–2050(2012), DOI(https://doi.org/10.1002/adma.201104634)

[5] M. Jayandran, M. Muhamed Haneefa, V. Balasubramanian, Green synthesis and characterization of Manganese nanoparticles using natural plant extracts and its evaluation of antimicrobial activity, J Appl Pharm , 5(12), 105–110(2015), DOI(https://doi.org/10.25271/sjuoz.2024.12.4.1384)

[6] H. Pan , X. Kong , P. Wen , T. Kitayama, and Q. Feng, Nanostructural evolution from nanosheets to one-dimensional nanoparticles for manganese oxide, Materials Research Bulletin, 47(9), 2428-2436(2012), DOI(https://doi.org/10.1016/j.materresbull.2012.05.035)

[7] R. N. Reddy, R. G. Reddy, Synthesis and electrochemical characterization of amorphous MnO2 electrochemical capacitor electrode material)), J Power Sources, N. 1-2, 132, 315–320(2004), DOI(10.1016/j.jpowsour.2003.12.054)

[8] S. Mitra, Y. Pak, N. Alaal, M.N. Hedhili, D.R. Almalawi, N. Alwadai, K. Loganathan, Y. Kumarasan, N. Lim, G.Y. Jung, I. S. Roqan, Novel P-Type Wide Bandgap Manganese Oxide Quantum Dots Operating at Deep UV Range for Optoelectronic Devices, Adv Opt Mater, 7(2), 1900801(2019), DOI(http://hdl.handle.net/10754/656556)

[9] S. Dawadi, A. Gupta, M. Khatri, B. Budhathoki, G. Lamichhane, N. Parajuli, Manganese dioxide nanoparticles: synthesis, application and challenges, Bull Mater Sci, 43(1), 5591(2020), DOI(10.1007/s12034-020-02247-8)

[10] M. M. Najafpour, S. I. Allakhverdiev, Manganese compounds as water oxidizing catalysts for hydrogen production via water splitting: From manganese complexes to nano-sized manganese oxides, Int J Hydrogen Energy, 37(10), 8753–8764(2012), DOI(https://doi.org/10.1016/j.ijhydene.2012.02.075)

[11] V. Štengl, D. Králová, F. Opluštil, T. Neˇmec, Mesoporous manganese oxide for warfare agents degradation, Microporous Mesoporous Mater, 156. 224– 232(2012), DOI(https://doi.org/10.1016/j.micromeso.2012.02.031)

[12] H. T. Zhang, X. H. Chen, J. H. Zhang, G. Y. Wang, S. Y. Zhang, Y. Z. Long, Z. J. Chen, N. L. Wang, Synthesis and characterization of one-dimensional $K0.27MnO_20.5H_2O$, J Cryst Growth, 280(1-2), 292–299(2005), DOI(https://doi.org/10.1016/j.jcrysgro.2005.02.063)

[13] Q. Shu-yan, F. Jing, Y. Jun, Hydrothermal synthesis and supercapacitor properties of urchin sphere and nanowire MnO_2, Chinese J Nonferrous Met, 18, 113–117(2008), DOI(10.1016/j.materresbull.2011.11.023)

[14] H. Yin, X. Dai, M. Zhu, F. Li, X. Feng, F. Liu, ((Fe-doped cryptomelane synthesized by refluxing at atmosphere: Structure, properties and photocatalytic degradation of phenol)), J Hazard Mater, Vol. 296, PP. 221–229(2015), DOI(https://doi.org/10.1016/j.jhazmat.2015.04.055)

[15] K. S. Shaker, A. H. Abdalsalm, Characterization Nano Structure of MnO_2 via Chemical Method, Eng Technol J, 36(9), 946–950(2018), DOI(https://doi.org/10.1016/j.matpr.2021.03.528)

[16] S. Sharma, P. Chauhan, and S. Husain Structural and optical properties of Mn2O3 nanoparticles & its gas sensing applications, 2(1), 220-220(2016), DOI(10.5185/amp.2016/220)

[17] K. H. Harbbi S. S. Jahil , ((Study the Lattice Distortion and Particle Size of One Phase of MnO by Using Fourier Analysis of X-ray Diffraction Lines)) University of Baghdad, 65, 2224-2225 (2016)

[18] K. H. Harbbi and S S. Jahil, Study the Lattice Distortion and Particle Size of One Phase of MnO by Using Fourier Analysis of X-ray Diffraction Lines, University of Baghdad, 65, 6-22 (2017)

[19] A. Hussain, A. Begum, and A. Rahman, Electrical and optical properties of nanocrystalline lead sulphide thin films prepared by chemical bath deposition, Indian Journal of Physics, 86(8), 697-701(2012), DOI(https://doi.org/10.23918/eajse.v8i2p10)

[20] A. D. Khalajia, M. Ghorbanib, Mn_2O_3 Nanoparticles Synthesized from Thermal Decomposition of Manganese(II) Schiff Base Complexes, Acta Physica Polonica A, 133(1), 133(2018), DOI(10.12693/APhysPolA.133.7)

[21] M. S. Niasari , M. E. Zare, and M. G. Daghian, Synthesis and characterization of Mn_2O_3 nanorods using a novel manganese precursor, 25(3), 879-884(2014), DOI(https://doi.org/10.1016/j.apt.2014.01.007)

[22] T. Mounika , Sh. L. Belagali, and K.T. Vadiraj, Manganese oxide nanoparticles synthesis route, characterization and optical properties, Materials Today: Proceedings, 75, 72–76(2023), DOI(https://doi.org/10.1016/j.matpr.2022.11.017)

[23] M. Sharrouf1, R. Awad, M. Roumié, and S. Marhaba, Structural, Optical and Room Temperature Magnetic Study of Mn2O3 Nanoparticles, IOP Conf. Series: Journal of Physics: Conf. Series, 6, 850-859 (2015), DOI(10.4236/msa.2015.610087)